Bispecific Antibody Pretargeting of Radionuclides for Immuno–Single-Photon Emission Computed Tomography and Immuno–Positron Emission Tomography Molecular Imaging: An Update

Robert M. Sharkey,[1] Habibe Karacay,[1] William J. McBride,[2] Edmund A. Rossi,[3] Chien-Hsing Chang,[3] and David M. Goldenberg[1]

Abstract Molecular imaging is intended to localize disease based on distinct molecular/functional characteristics. Much of today's interest in molecular imaging is attributed to the increased acceptance and role of ^{18}F-flurodeoxyglucose (^{18}F-FDG) imaging in a variety of tumors. The clinical acceptance of ^{18}F-FDG has stimulated research for other positron emission tomography (PET) agents with improved specificity to aid in tumor detection and assessment. In this regard, a number of highly specific antibodies have been described for different cancers. Although scintigraphic imaging with antibodies in the past was helpful in patient management, most antibody-based imaging products have not been able to compete successfully with the sensitivity afforded by ^{18}F-FDG-PET, especially when used in combination with computed tomography. Recently, however, significant advances have been made in reengineering antibodies to improve their targeting properties. Herein, we describe progress being made in using a bispecific antibody pretargeting method for immuno–single-photon emission computed tomography and immunoPET applications, as contrasted to directly radiolabeled antibodies. This approach not only significantly enhances tumor/nontumor ratios but also provides high signal intensity in the tumor, making it possible to visualize micrometastases of colonic cancer as small as 0.1 to 0.2 mm in diameter using an anti–carcinoembryonic antigen bispecific antibody, whereas FDG failed to localize these lesions in a nude mouse model. Early detection of micrometastatic non–Hodgkin's lymphoma is also possible using an anti-CD20–based bispecific antibody pretargeting procedure. Thus, this bispecific antibody pretargeting procedure may contribute to tumor detection and could also contribute to the detection of other diseases having distinct antigen targets and suitably specific antibodies.

Antibody Targeting

A variety of imaging methods are used for cancer detection, and although they are usually not sufficiently specific to be used diagnostically, their role in accurate staging and monitoring treatment responses are key elements in cancer management. X-ray methods, most commonly computed tomography, are the most widely used anatomic-based imaging methods, but magnetic resonance imaging, ultrasound, and scintigraphic scans are also used in specific settings (1–5). With the advent of ^{18}F-fluorodeoxyglucose (^{18}F-FDG) positron emission tomography (PET), nuclear imaging has become an increasingly common procedure for detecting a number of cancers, contributing to diagnosis, staging, and monitoring therapy (6). Nuclear imaging differs from traditional anatomic imaging methods because it relies on functional characteristics of the malignant cells that provide a more selective uptake of the radiotracer by the target, such as higher glycolysis rates in tumors that gives FDG its relative specificity (proliferating inflammatory cells also show this property, however). The fusion of functional PET imaging with the anatomic orientation provided by computed tomography is becoming increasingly recognized as an established procedure in the detection and assessment of a number of cancer types (7, 8). Also, there are a growing number of new molecular probes being developed for PET imaging; however, their role in cancer detection and management remains to be assessed (5).

Antibodies are of interest as molecular imaging agents because they are highly specific and can be developed against just about any antigen (5). Conceivably, they could be used with greater diagnostic certainty than ^{18}F-FDG if they can discriminate cancer from inflammation or other structures that are avid for FDG. Indeed, radiolabeled antibodies were widely

Authors' Affiliations: [1]Garden State Cancer Center, Center for Molecular Medicine and Immunology, Belleville, New Jersey; and [2]Immunomedics, Inc., and [3]IBC Pharmaceuticals, Inc., Morris Plains, New Jersey

Received 5/7/07; accepted 5/16/07.

Grant support: National Cancer Institute grant P01 CA103985 and New Jersey Department of Treasury grant CDG-06-103.

Presented at the Eleventh Conference on Cancer Therapy with Antibodies and Immunoconjugates, Parsippany, New Jersey, USA, October 12-14, 2006.

Note: W.J. McBride, E.A. Rossi, C-H. Chang, and D.M. Goldenberg declare employment and/or stock interests in Immunomedics and IBC Pharmaceuticals, which have developed some of the reagents described in this review. The other authors declare no potential competing financial interests.

Requests for reprints: Robert M. Sharkey, Garden State Cancer Center, Center for Molecular Medicine and Immunology, 520 Belleville Avenue, Belleville, NJ. Phone: 973-844-7121; Fax: 973-844-7120; E-mail: rmsharkey@gscancer.org.

doi:10.1158/1078-0432.CCR-07-1087

investigated as imaging agents before the advent of ^{18}F-FDG-PET, and several agents received Food and Drug Administration approval for human use to aid in the detection of ovarian, colorectal, lung, and prostatic cancers (9–15). However, ^{18}F-FDG-PET's high sensitivity and good resolution for disclosing many cancers has since replaced most of these earlier agents (all of which were for use only for single-photon emission computed tomography and not PET imaging), with only capromab pendetide, an ^{111}In-labeled antibody to prostate cancer (10, 14), remaining in clinical use because ^{18}F-FDG has not been successful in identifying prostatic cancer (16). In many respects, the high-contrast images acquired with ^{18}F-FDG-PET, which are in stark difference to the low contrast images most often obtained with antibodies, have set a standard against which new agents are measured.

The poor contrast obtained with radiolabeled antibodies is due to low tumor uptake combined with insufficient clearance from surrounding tissues. IgG and its fragments have very different characteristics that define their targeting properties, from how quickly they reach the target antigen and clear from the blood, which organ is principally involved in their removal from the blood, how well they penetrate into the tumor bed, and how much of the injected product will bind to the target. Once antibodies come into contact with the intended target, they generally bind with high avidity, which holds the antibody in place for a period of time, whereas the unbound antibody is processed by various organs in the body. An IgG clears very slowly from the blood, requiring several days before a sufficient amount is removed from the circulation to allow the specific concentration taken into the tumor to be revealed. Its slow clearance is in part due to its large size, ~150,000 kDa, that impedes its percolation from inside the vascular channels to the extravascular space, giving an IgG its characteristic slow accretion in tumors.

Because the concentration of an IgG remains high in the vascular compartment and the vascular channels of a tumor are leakier than most normal tissues (17, 18), the IgG is slowly (i.e., 1-2 days) able to achieve a relatively high concentration in tumors. In mouse xenograft models, tumor uptake is typically between 10% and 30% of the injected activity per gram tumor; however, in humans, with the larger vascular and extravascular volume of distribution, this accretion is typically reduced to <0.1% per gram (19, 20). As the molecular size of an antibody is reduced from divalent F(ab′)2 fragment (~100 kDa) to a monovalent binding Fab′ fragment (~50 kDa), there is progressively faster clearance from the blood. Higher tumor/blood ratios are obtained, but generally at the cost of having proportionally less of the injected product reaching the tumor (21, 22). Molecular engineering has enabled the formation of smaller antibody fragments, such as scFv (~25 kDa), that are cleared even more rapidly from the blood and with progressively less uptake in tumors (23). There are even smaller nanobodies, affibodies, and synthetically created binding molecules, known as selective high-affinity ligands, that are being evaluated for targeting strategies (24–26).

Molecular manipulation of antibodies revealed that molecular size alone was not the only factor governing antibody clearance. By deleting the CH2 sequence of an IgG, the resulting construct, although still divalent and nearly 100 kDa in size, cleared extraordinarily quickly from the blood, yielding excellent localization ratios within a short period (27). Others have site-specifically mutated the neonatal Fc receptor–binding region of the Fc, which regulates the pharmacokinetic behavior of antibodies, to create new constructs with more rapid blood clearance properties and enhanced tumor visualization (28, 29). Although the exceedingly rapid clearance properties of scFv with low tumor accretion are generally considered pharmacokinetically unfavorable for targeting radionuclides, a number of innovative strategies have been undertaken to restore in part the multivalency of an antibody to enhance tumor retention. This resulted in a higher molecular size, allowing the construct to clear from the blood slower than a scFv, but more quickly than an IgG. These constructs, ranging from divalent diabodies, minibodies $(scFv)_2$-Fc, and other assorted constructs, are essentially composed of multiple scFvs held tethered in different ways (30, 31).

Most radiolabeling methods attach the radionuclide to the antibody in a very stable manner, and thus the radionuclide is carried throughout the body attached to the antibody. Radionuclides can be stripped from the antibody while in the blood, but it is more likely that the radionuclide is separated from the antibody through catabolic processes that occur within the microenvironment of a tissue or tumor, or when taken inside cells. Once liberated from the antibody, the fate of the radionuclide is dictated by its properties. Radioiodine is taken up and retained by the thyroid, but the majority is eliminated by both gastrointestinal and urinary excretion, whereas radiometals can bind to various serum proteins and tend to be retained by certain tissues within the body, including reticuloendothelial cells, renal tubules, or cortical bone, to mention a few (21, 32–36). This property can be used to the advantage of antibodies that, as a consequence of their binding to the tumor cell surface, will become internalized, trapping the radiometal inside the cell. In contrast to radiometals, radioiodine, linked to antibodies by the more common tyrosine-coupling radiolabeling procedures, is not retained by cells, but is released and ultimately removed from the body or taken up by the thyroid. However, radioiodine can be attached to antibodies by other methods that will retain the radioiodine in a cell for a longer period of time (37, 38). Thus, the properties of radionuclide dictate its fate when it is released from the antibody, but it is the properties of the antibody (i.e., its molecular size, charge, or even its specificity) that determine which tissue affects isotope catabolism. As a general rule, IgG and constructs that are typically >60 kDa are catabolized primarily in the liver, whereas smaller constructs are filtered from the blood directly in the kidneys and excreted via the urine. Because radioiodine is not retained when catabolized in these tissues, it is often the preferred radionuclide for antibodies. In this regard, ^{123}I-labeled (single-photon emission computed tomography) and ^{124}I-labeled (PET) antibodies have been used successfully (39–48). Uptake of a radiometal-labeled antibody fragment in the kidneys can be as much as 10-fold higher than that in the tumor, which makes interpretation in this region challenging (22, 32, 49–51). Tumors have been revealed in the liver with radiometal-labeled antibodies because they are visualized as "cold spots" against the higher uptake in the uninvolved liver (52, 53). Specialized linkage chemistries that enable the chelated radiometal to be removed from the normal liver by organ-specific enzymes improve tumor/liver ratios (54), but do not prevent substantial accretion and retention of a radiometal-labeled IgG by the liver. There have also been techniques for reducing renal retention of

radiometal-labeled antibody fragments (22, 55–57), but none of these methods can prevent renal build-up sufficiently so that tumor uptake exceeds that found in the kidneys. High tissue retention does not discount the use of a radiometal-labeled IgG for cancer detection in the chest or pelvis, or the use of antibody fragments for detecting hepatic metastases, as well as other regions not obscured by the kidneys; however, antibody imaging methods would benefit if the whole body could be examined in one study, as well as from improvements in signal strength and the reduction of background noise. Thus, although several interesting antibody constructs have shown promising targeting properties as radioiodinated products (51, 58–60), none has fully overcome the limitations found when the radionuclide is directly attached to the antibody.

Pretargeting

Solving the problem associated with the deficiencies in targeting with directly radiolabeled antibodies requires an entirely different method involving separating the targeting of a slowly clearing antibody from a rapidly clearing radiometal-chelate complex. To accomplish this, a bispecific antibody (bsMAb) was developed that had the ability to bind to a target antigen as well as the radiometal-chelate complex (61, 62). Bispecific antibodies were first made by chemically linking a Fab′ fragment of an antitumor antibody to a Fab′ fragment of the antichelate antibody. Today, the process of preparing bsMAb is done more efficiently through molecular engineering (63–65). Pretargeting evolved over time to its current form, where the bsMAb is given sufficient time to localize in the tumor and clear from the blood before the radiometal-loaded chelate is administered. The radiometal-loaded chelate has excellent clearance properties. The vast majority is removed from the blood in less than an hour with minimal retention in normal tissues, even the kidneys, where most of the product passes as it is removed from the body by urinary excretion. Just as important, its small size enables it to quickly enter the extravascular space of a tumor, where, when encountering the antichelate binding arm of the bsMAb, it is trapped, while the remaining material is flushed from the body rapidly. This procedure allows for rapid radionuclide uptake in the tumor and considerably improved tumor/blood ratios.

The first clinical testing of a bsMAb pretargeting method for cancer imaging reported successful localization of colonic cancer metastases in the liver using an ^{111}In-chelate complex given 5 days after the administration of an unlabeled anti-carcinoembryonic antigen (CEA) × antichelate bsMAb (66). In contrast, an ^{111}In-labeled antibody to colorectal cancer had excessive amounts of ^{111}In in the liver that frequently masked tumor targeting (52, 53, 67, 68). Thus, the pretargeting approach was viewed as a successful alternative to attaching the radionuclide directly to an antibody.

Initially, pretargeting used the chelate-radiometal complex by itself, but LeDoussal et al. (69) found that by chemically coupling two chelates [e.g., diethylenetriaminepentaacetic acid (DTPA)] to an amino acid backbone, thereby creating a bivalent "hapten" (i.e., DTPA-Lys-Tyr-DTPA) that could be radiolabeled, the radioactivity bound more stably at the tumor site, presumably because the divalent hapten-peptide could be cross-linked by two adjacent bsMAbs (Fig. 1). This innovation became known as the affinity enhancement system, which was later confirmed by others (70, 71). An anti-CEA × anti-DTPA(In) bsMAb was used successfully to target CEA-producing tumors in patients with an ^{111}In- or ^{131}I-labeled di-DTPA peptide (72–74). Because pretargeting approaches were considered to be complex, requiring careful adjustment of a number of variables, and tumor targeting required several days for the unlabeled bsMAb to localize in the tumor before the radiolabeled hapten could be given, this technique was largely disregarded for imaging applications when antibody Fab′ fragments directly radiolabeled with ^{99m}Tc were introduced (12, 13).

Can Pretargeting Provide a New Paradigm for Antibody-Based Molecular Imaging?

Pretargeting procedures have accomplished what molecular engineering continues to strive for in the design of antibody molecules; namely, the high tumor uptake advantage of a directly radiolabeled IgG with the rapid blood clearance of an

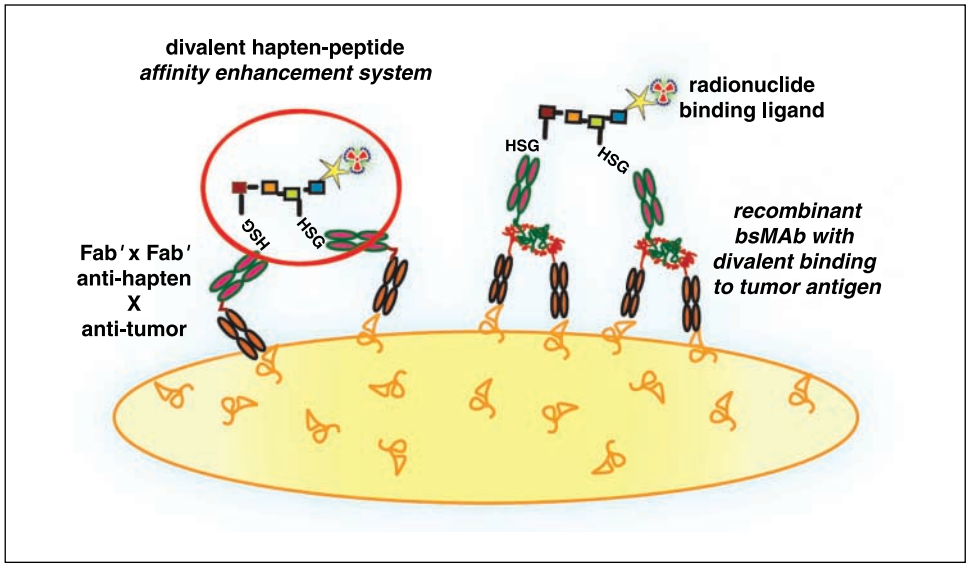

Fig. 1. Schematic of bsMAb binding to tumor cells cross-linked with a divalent hapten-peptide that can improve retention of the radiolabeled hapten-peptide by a process known as the affinity enhancement system. The HSG hapten-binding system allows the peptide portion to be modified to accommodate different types of radionuclide-binding ligands or other compounds while still retaining its ability to bind to the anti-HSG portion of the bsMAb. Bispecific antibodies historically have been formed by chemically linking a Fab′ of the antitumor antibody to the Fab′ of an anti-hapten antibody, but bsMAb are now more commonly prepared as recombinant proteins. Divalent binding to the tumor antigen can also improve uptake and retention of the bsMAb.

antibody fragment. Although pretargeting methods are more complicated than a single-agent targeting method, once the optimal conditions are established, the injection sequence is straightforward. Irrespective of the pretargeting method used, patients would be able to receive the injection of the bsMAb or antibody conjugate by their oncologist, and then return a few days later to receive the radiolabeled product in a nuclear medicine facility. Imaging could be done on the same day, within a few hours of this injection. Thus, for a pretargeting procedure, it will take a few days before an image is acquired, whereas it may be possible with some of the smaller, directly radiolabeled antibody constructs to image in a shorter period of time. However, in our experience, preclinical data suggest that image quality with a pretargeting procedure will be superior to that of a directly radiolabeled antibody fragment (75, 76).

Recent results with pretargeting. To assess the utility of pretargeting for molecular imaging, we initiated several projects that compared a bsMAb-based pretargeting to directly radiolabeled antibody fragments, as well as to the currently accepted gold standard of ^{18}F-FDG-PET. We have emphasized a pretargeting approach based on bsMAbs primarily because the bsMAb can be humanized, reducing the potential for an anti-antibody response that could limit the number of times an imaging procedure could be used, including the later application of the same agents for therapy. We have reported a number of novel recombinant bsMAbs, with molecular sizes ranging from ~50 to 157 kDa (63–65). Each construct has done exceptionally well in a pretargeting setting. We have focused on constructs with the ability to bind divalently to the tumor target antigen and monovalently to the hapten-peptide, because these constructs showed improved tumor uptake and retention of the radiolabeled hapten-peptide (64, 77). The bsMAb pretargeting system of current interest is based on a unique hapten-binding system that provides greater flexibility for inserting hapten-peptides, with the capability of carrying a variety of different radionuclides (78). The anti-hapten antibody is based on the murine 679 MAb that reacts with high affinity (e.g., 10^{-9} mol/L) to histamine-succinyl-glycine (HSG). Following the principles of the affinity enhancement system, two HSG residues are inserted within an amino acid backbone that can also be linked to chelates for specific and stable binding of radiometals, with tyrosine for radioiodination, or with ligands capable of binding other compounds of imaging or therapeutic interest. We have used di-HSG-peptides capable of binding ^{111}In, ^{90}Y, ^{177}Lu, ^{99m}Tc, ^{188}Re, and ^{131}I, ^{125}I, and ^{124}I (75, 78, 79). The composition of the amino acids can be varied to impart favorable charge and hydrophilic properties to the di-HSG-peptide that encourage renal over hepatic excretion; D-amino acids are used to improve plasma stability.

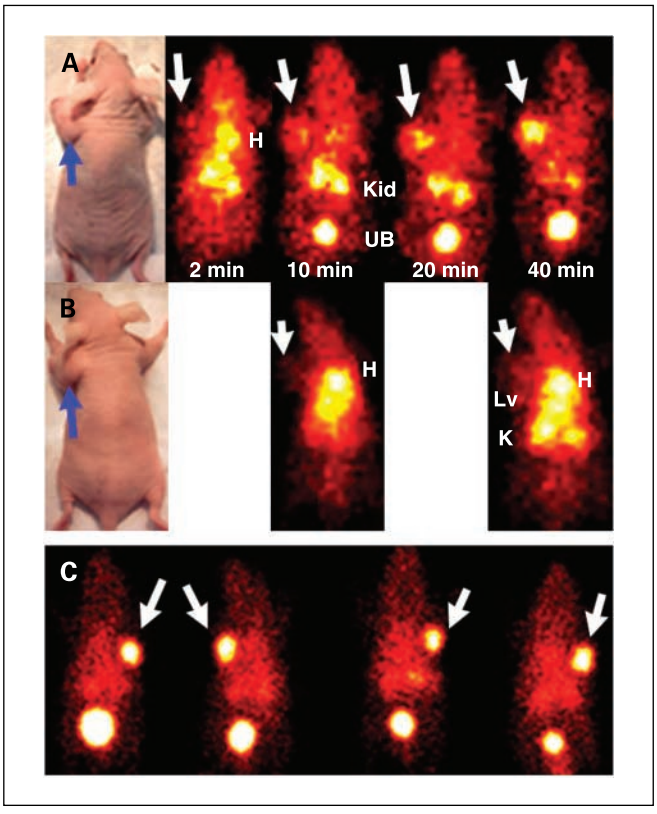

Fig. 2. Enhanced tumor targeting using a bsMAb pretargeting procedure with a ^{99m}Tc-labeled hapten-peptide. *A* and *B*, two nude mice bearing ~1.2 g human colonic tumor xenografts (*blue arrow*). The animal in (*A*) was given an anti-CEA bsMAb 2 d in advance of the ^{99m}Tc-labeled hapten-peptide, whereas the animal (*B*) was given ^{99m}Tc-anti-CEA Fab′. Dynamic imaging at 2-min intervals over 60 min revealed tumor localization of the ^{99m}Tc-hapten-peptide in the pretargeted animal within 10 min. Tumor uptake exceeded uptake in other tissues within 40 min, with most of the ^{99m}Tc excreted in the urine. In contrast, the ^{99m}Tc-Fab′ remained in the blood pool and major organs with no evidence of enhanced uptake in the tumor in this same period of time. The four animals shown in (*C*) had ≤0.2 g human colonic xenografts and were pretargeted with the anti-CEA bsMAb 1 d before the ^{99m}Tc-hapten-peptide was given. The images show clear localization of the tumors within 1 h of the ^{99m}Tc-hapten-peptide injection. H, heart; Kid, K, kidneys; UB, urinary bladder; Lv, liver.

For the most part, we have continued to focus on anti-CEA antibody pretargeting systems, and in the first series of studies, explored the possibility that a pretargeting approach with anti-CEA bsMAb pretargeting could outperform direct targeting with the ^{99m}Tc-labeled anti-CEA Fab′ fragment approved for imaging colorectal cancer metastases, arcitumomab (76). Dynamic imaging studies showed that in nude mice bearing a subcutaneous human colonic cancer xenograft, a ^{99m}Tc-labeled di-HSG-peptide was accreted quickly into the tumor, and if pretargeted with an anti-CEA bsMAb, tumor uptake became higher than in the heart within 20 min, and within 40 min it was higher than in the kidneys (Fig. 2). About 60% of the injected activity could be accounted for in the urinary bladder within 1 h, indicating the rapid removal from the body. In contrast, the ^{99m}Tc-Fab′ showed no evidence of selective tumor localization within 1 h, and even by 24 h, tumor/blood ratios for the ^{99m}Tc-Fab′ were just 3.8 ± 0.9, whereas in the pretargeted animals, tumor/blood ratios had exceeded this level within 1 h (8.6 ± 3.7), and by 6 h, reached an average of ~70:1. ^{99m}Tc-Fab′ activity in the kidneys was 20-fold higher than in the tumor, whereas for the pretargeted ^{99m}Tc-labeled peptide, tumor uptake was 5-fold higher than in the kidneys. Tumor uptake from the pretargeted ^{99m}Tc-labeled peptide was 2- to 3-fold higher than with the ^{99m}Tc-anti-CEA Fab′. Tumors as small as 5 mm in diameter were easily visualized in the pretargeted animals within 1 h. These studies illustrated the superior targeting capability of this pretargeting method over that of a conventional, clinically proven, ^{99m}Tc-anti-CEA Fab′ imaging agent for colorectal cancer.

To assess the capabilities of this procedure for PET imaging, radioiodination techniques were developed so the peptide could be labeled with ^{124}I (75). High-specific-activity, clinical

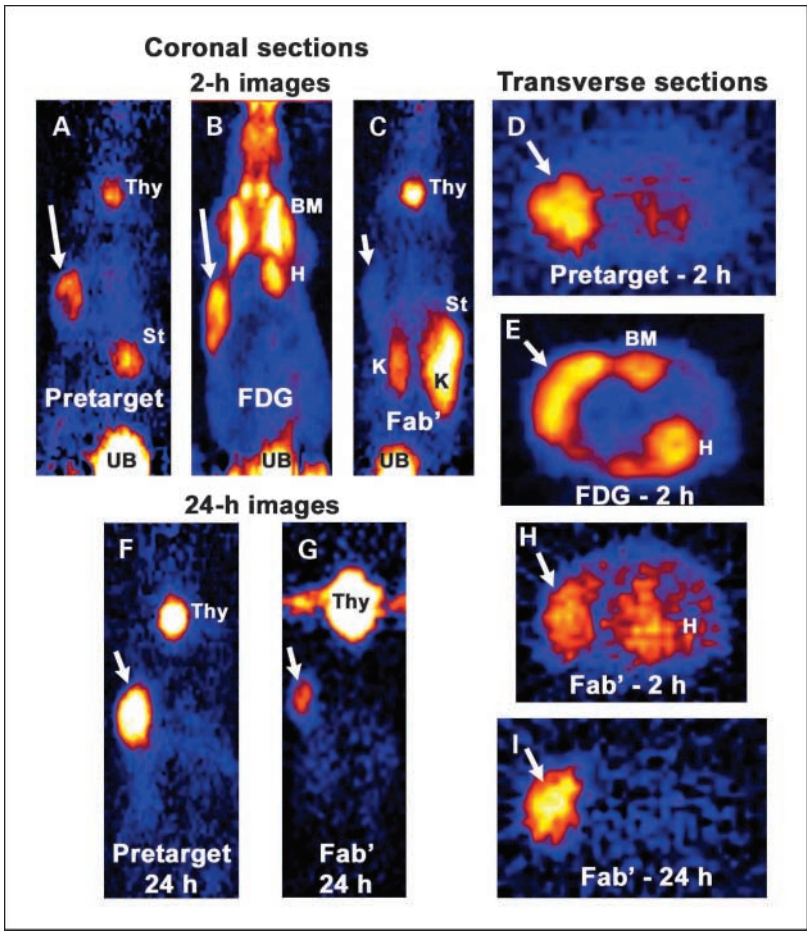

Fig. 3. MicroPET imaging of nude mice bearing s.c. LS174T human colonic tumors in the upper left flank comparing pretargeting (anti-CEA bsMAb with an ^{124}I-labeled hapten-peptide) to ^{18}F-FDG and an ^{124}I-anti-CEA Fab′. Animals given ^{124}I were not premedicated to reduce thyroid (*Thy*) or gastric uptake. Coronal slices (*A-C*) show clear evidence of tumor uptake (*arrows*) in the pretargeted (*A*) and the ^{18}F-FDG animal (*B*) 2 h after injection, but not in the ^{124}I-Fab′ animal primarily because of the much higher accretion in the stomach (*St*) and kidneys. By 24 h, uptake in the normal tissues had decreased sufficiently so that the tumor could be appreciated in the coronal and transverse sections of the ^{124}I-Fab′ (*G* and *I*, respectively), but the pretargeted tumor had a more intense signal (*F*). Although the tumor could be visualized with ^{18}F-FDG (*B*), high uptake in the bone marrow (*BM*; scapula), heart wall, and brain was also seen. Transverse sections through the upper body cavity in the plane of the tumor show tumor targeting was apparent in all animals, albeit uptake in the pretargeted animal (*D*) showed less activity in the heart than the ^{124}I-Fab′ (*H*), and the ^{18}F-FDG had elevated activity in the heart wall, spinal column, and ribs (*E*).

grade ^{124}I is commercially available, and although ^{124}I does not have as favorable emissions as ^{18}F, delayed imaging (e.g., 6-24 h after injection) would be possible because of its longer half-life (4.2 days versus ~110 min for ^{18}F). Delayed imaging would give time for the radionuclide to be excreted from the urinary bladder, allowing unobstructed views of the lower pelvis (e.g., for prostate cancer imaging), as well as enhance the confidence in image interpretation for signals that remain

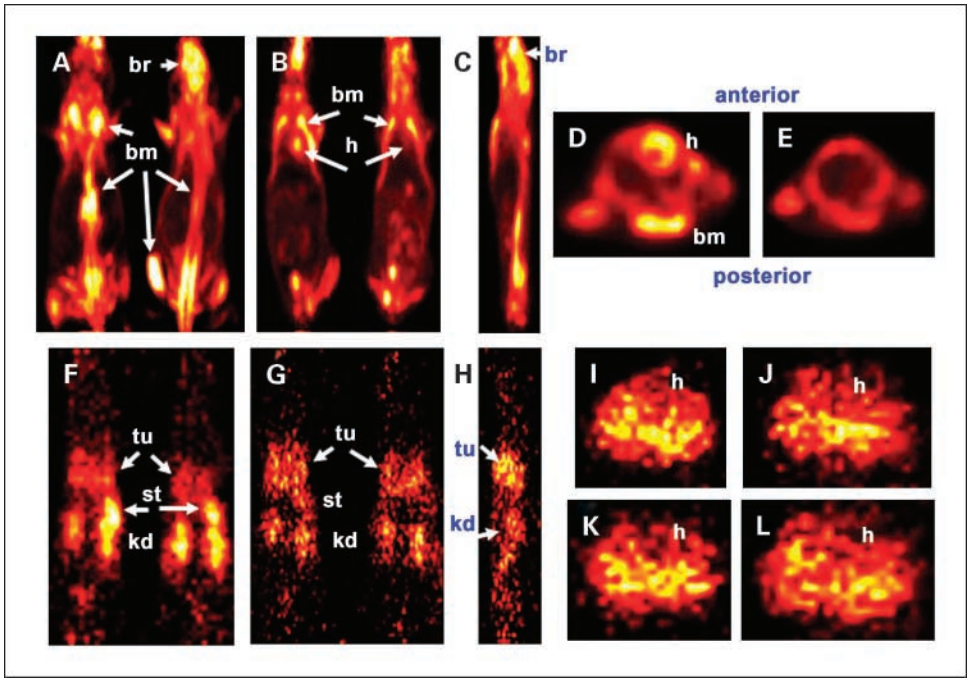

Fig. 4. MicroPET images of nude mice injected i.v. with a human colon cancer cell line, and bearing multiple (~80 to 120) microscopic (~0.1 to 0.2 mm) tumor colonies in the lungs. Top, images of animals 1.0 h after the injection of ^{18}F-FDG. *A* and *B*, coronal sections (*A* is more posterior than *B*); *C,* a central sagittal section; *D* and *E,* transverse sections through the chest of two animals. These images show intense uptake in the brain (*br*), bone marrow (*bm*), and heart wall (*h*), but no evidence of uptake in the chest to suggest tumor (*tu*) involvement. Bottom (*F-L*), two animals that were first given an anti-CEA bsMAb and 22 h later received an ^{124}I-hapten-peptide. The images, taken 1.5 h after injection of the ^{124}I-hapten-peptide, show clear evidence of localization of tumor (*tu*) in the lungs on all coronal (*F* and *G*), sagittal, and transverse sections. Tumor uptake remained as strong 1 d after the ^{124}I-hapten-peptide injection (*K* and *L*) as seen at 1.5 h (*I* and *J*). st, stomach; kd, kidney.

strong. Other radionuclides with somewhat more favorable imaging properties, such as ^{68}Ga and ^{64}Cu, also could be adopted for pretargeted imaging. The radioiodinated di-HSG-peptide was prepared with a high level of purity, and when used in a pretargeting setting, it had similar tumor uptake and tissue distribution as the ^{111}In-labeled version of this same hapten-peptide, with the exception that the iodinated hapten-peptide had higher stomach and thyroid uptake in mice that were not premedicated to reduce iodide uptake in these tissues. In nude mice bearing a subcutaneous human colonic tumor xenograft, within 1 h of the radioiodinated hapten-peptide injection, tumor/blood ratios averaged 10:1, with tumor/kidney ratios averaging 3.4 ± 1.3 (75). Comparisons were then made in nude mice given the pretargeted ^{124}I-hapten-peptide to animals given ^{18}F-FDG and animals given ^{124}I-anti-CEA Fab′. MicroPET imaging was used to visualize uptake and distribution (Fig. 3). Necropsy and regions of interest data confirmed that the pretargeting method has superior tumor uptake (15.4 ± 3.1% versus 4.8 ± 1.1% ID/g at 1 h postinjection for the pretargeting and ^{18}F-FDG animals, respectively) and improved tumor/nontumor ratios for most tissues compared with ^{18}F-FDG (tumors were visualized in each group of animals 1-2 h after injection). In mice, ^{18}F-FDG had highly elevated uptake in the bone marrow, heart wall, and brain, whereas none of these tissues was visualized with the pretargeted ^{124}I-hapten-peptide. Delayed imaging 1 day after the ^{124}I-hapten-peptide injection showed that the tumor had retained its strong signal, with no activity remaining in any other tissue, except the thyroid, which had not been blocked. Tumor visualization in coronal whole-body sections was difficult with the ^{124}I-anti-CEA Fab′, because of excessive activity in the kidneys and stomach through 24 h (75). Unlike the ^{99m}Tc-anti-CEA Fab′, where high renal uptake persisted over 24 h, renal uptake with the ^{124}I-Fab′, although highly elevated initially, diminished significantly over time, so that its uptake in the kidneys was lower than that seen with the pretargeted ^{124}I-hapten-peptide at 24 h (0.4 ± 0.2% versus 2.7 ± 0.3% ID/g, respectively). However, tumor uptake of the ^{124}I-Fab′ also decreased from its maximum of ~5% to 0.8 ± 0.2% ID/g, whereas tumor uptake in the pretargeted animals remained high (12.5 ± 1.1% ID/g), thereby providing a 15-fold improvement in signal strength at the tumor. Thus, in this series of studies, pretargeting provided less ambiguous imaging of the s.c. colonic cancer xenograft than ^{18}F-FDG or ^{124}I-Fab′ due to enhanced tumor uptake and tumor/nontumor ratios (75).

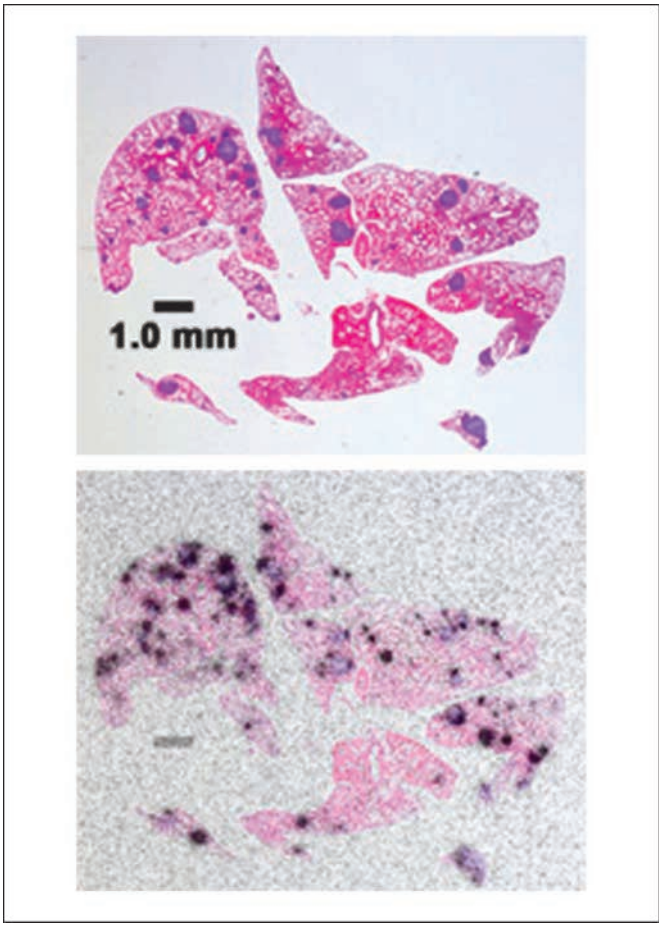

Fig. 5. Autoradiographic evidence of selective uptake of a pretargeted ^{111}In-labeled hapten-peptide in the individual tumor nodules found in the lungs of nude mice given an i.v. injection of a human colon cancer cell line. Three weeks after tumor inoculation, a nude mouse was injected with the anti-CEA bsMAb and the next day, the animal was given an ^{111}In-labeled hapten-peptide. Three hours later, the lungs were removed and fixed in formalin for 2 h, and sections were placed on X-ray film. Fourteen days later, the film was developed, which revealed highly specific uptake in the individual tumor nodules (*bottom*). Top, the H&E-stained cross-section of a lung showing several visible (≤5 mm) tumor colonies. Bottom, overlay of the autoradiography film on the H&E-stained section to illustrate the uptake corresponding to colonies seen.

To challenge the imaging ability of the pretargeting method further, we turned to a micrometastasis model of a human colonic cancer xenograft that we described earlier (80). A tumor suspension injected i.v. leads to the formation of small tumor nodules exclusively within the lungs. In this study, animals were imaged 1 to 3 weeks after tumor inoculation (81). Histology sections of the lungs taken from these animals between 7 and 11 days after implantation showed multiple (80-120) tumor colonies, most being between 0.1 and 0.2 mm in diameter, and by 3 weeks, the colonies were ≤0.5 mm in diameter. A pretargeted ^{111}In- or ^{99m}Tc-labeled di-HSG-peptide showed localization of the lungs in tumor-bearing animals 1 week after inoculation, but no uptake was seen in the lungs of non–tumor-bearing animals. Necropsy data showed ~9-fold higher uptake in the tumor-bearing lungs than non–tumor-bearing lungs with pretargeting just 1 h after the ^{99m}Tc-peptide injection. The tumor nodules within the lungs were too small to dissect free from the lung tissue to obtain a direct measure of uptake, but comparison of the weights of tumor-bearing and non–tumor-bearing lungs suggested that the total tumor mass in the lungs was between 10 and 50 mg. The percentage uptake of ^{18}F-FDG in tumor-bearing lungs was similar to that seen with the anti-CEA bsMAb pretargeted ^{99m}Tc-peptide, but uptake in tumor-bearing lungs was only 1.5-fold higher when compared with non–tumor-bearing lungs with ^{18}F-FDG and the ^{99m}Tc-peptide alone. Thus, pretargeting provided a more highly specific uptake in the tumor-bearing lungs than in the non–tumor-bearing lungs than the peptide alone or ^{18}F-FDG. MicroPET imaging studies of nude mice bearing 0.1 to 0.2 mm tumor nodules in the lungs failed to reveal any evidence of targeting with ^{18}F-FDG (Fig. 4A-E), ^{124}I-labeled peptide alone, or the ^{124}I-labeled peptide pretargeted with an irrelevant bsMAb (anti-CD22 × anti-HSG bsMAb), but within just 1 to 2 h after injection, tumor localization in the lungs with the anti-CEA bsMAb pretargeted ^{124}I-labeled peptide was

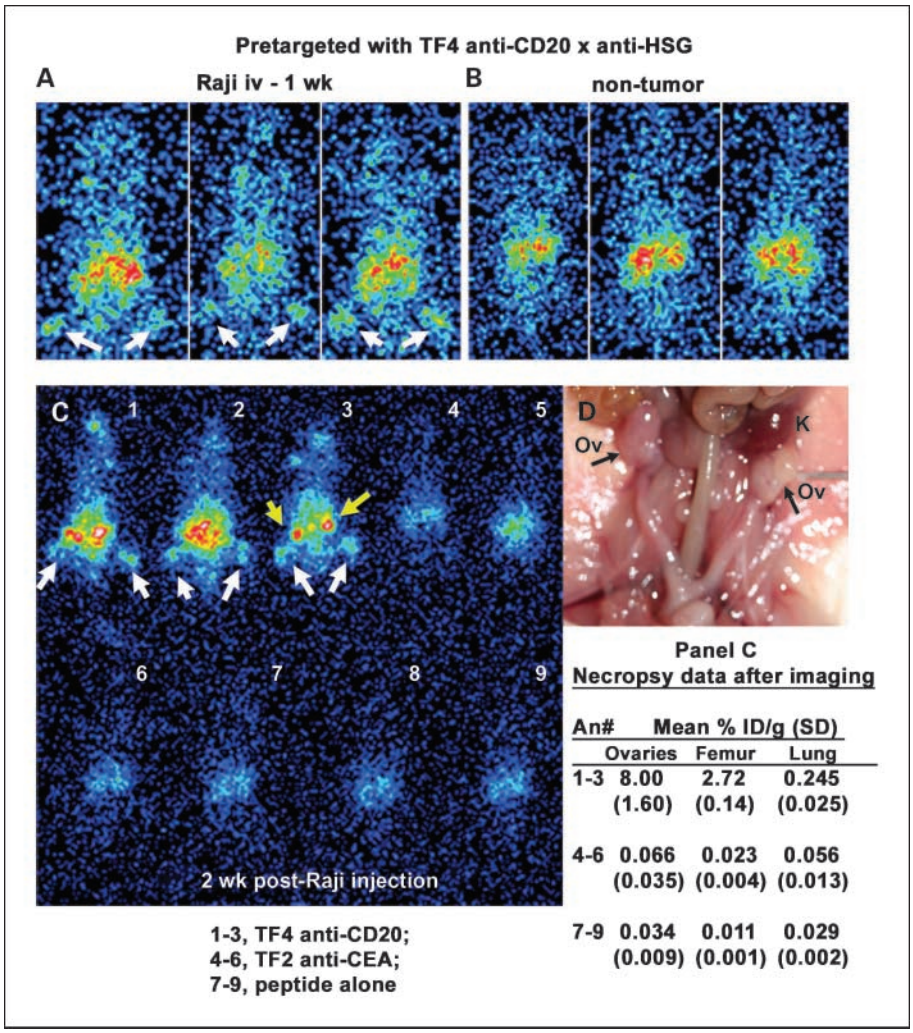

Fig. 6. Planar scintigraphy showing evidence of early lymphomatous involvement in SCID mice. Top, the three mice on the left (*A*) were injected i.v. with the Raji cell line, whereas the three animals to the right (*B*) did not receive tumor. One week later, these animals were given an i.v. injection of an anti-CD20 bsMAb (TF4). After allowing the bsMAb to clear from the blood, an ^{111}In-di-HSG-peptide was injected and animals were imaged 24 h later. Femur uptake (*arrows*) is seen in the tumor-bearing, but not the non – tumor-bearing animals. Uptake in the abdomen was similar in both sets of animals, despite tissue-counting data obtained following this imaging session that indicated ~10-fold higher uptake in the ovaries in the tumor-bearing mice compared with the non – tumor-bearing mice. *C,* the same pretargeting procedure was given to an additional set of animals 2 wk after tumor inoculation. The three animals given the TF4 anti-CD20 bsMAb followed by the ^{111}In-peptide showed selective targeting in the femurs (*white arrows*), abdomen (i.e., ovaries, *yellow arrow*), and in the upper body, whereas animals given the ^{111}In-labeled peptide alone or pretargeted by an irrelevant anti-CEA bsMAb had significantly lower uptake in these regions. Necropsy data from these animals evaluated after the 24-h imaging session showed from 10 to as much 100 times higher uptake in the TF4-pretargeted animals than in the control animals. *D,* necropsy photograph shows the location of the lymphomatous-involved enlarged ovaries (*Ov*) just below the kidneys (*K*).

evident (Fig. 4F-L). Indeed, there was even a suggestion that individual tumor nodules could be identified in the 24-h post-pretargeted peptide injection images. In agreement with the microPET imaging results, autoradiography studies revealed highly selective localization of tumor nodules within the lungs by the anti-CEA bsMAb pretargeted peptide (Fig. 5). Thus, in this model, pretargeting outperformed ^{18}F-FDG again, but in this case, ^{18}F-FDG gave false-negative results, whereas the positive targeting reading with the anti-CEA bsMAb pretargeting procedure was unmistakable, with controls confirming that the localization was highly specific.

The capability of this pretargeting procedure is not restricted to CEA-producing tumors. We have examined bsMAb that can localize other tumor-associated antigens, such as colon-specific antigen-p (78), a MUC-1 antigen that is highly specific for pancreatic cancer (82), and CD20 for targeting non – Hodgkin's lymphoma (83). Studies have been initiated to examine the capability of an anti-CD20 × anti-HSG bsMAb, prepared by the dock-and-lock method (63), to localize human lymphoma cells in SCID mice. Microdisseminated SCID mouse models of non – Hodgkin's lymphoma similar to the one described initially by Ghetie et al. (84) have been widely reported in the literature, and like the colonic cancer model, they represent an excellent challenge for pretargeting not only to assess early sites where the tumor begins to grow and spread, but potentially to monitor treatment response. Our initial goal has been to examine how early after tumor inoculation can tumor be detected in animals injected with several human B-cell lymphoma cell lines. We have found that within 3 weeks of an i.v. injection of the Raji human Burkitt's lymphoma cell line and 4 to 5 weeks of injection of the Ramos B-cell lymphoma cell in SCID mice (i.e., 2.5×10^5 cells), hind leg paralysis occurs. As shown in Fig. 6A and B, images comparing anti-CD20 – pretargeted tumor-bearing and non – tumor-bearing animals taken 1 week after tumor inoculation indicated uptake in femurs, which was subsequently confirmed at necropsy (0.502-0.683% ID/g versus 0.016-0.023% ID/g in the femurs of the tumor-bearing versus nontumor-bearing pretargeted animals). Necropsy data also indicated ovarian involvement (e.g., 0.64-1.7% ID/g in the ovaries of the three tumor-bearing animals versus 0.08-0.10% ID/g in the ovaries of the three non – tumor-bearing animals); however, the images could not definitively differentiate selective uptake in the ovaries compared with activity in the kidneys. At 2 weeks after tumor implantation (Fig. 6C), the comparison of tumor-bearing animals given the radiolabeled peptide alone or pretargeted with an irrelevant bsMAb (anti-CEA) to those obtained in animals given the specific anti-CD20 bsMAb

showed enhanced uptake in the femurs, but also strong tracer uptake in the pelvis. Necropsy data identified the pelvic activity as uptake in the ovaries, which, as shown in Fig. 6D, were enlarged and located below the kidneys. Necropsy data also suggested that there was higher uptake in the lungs compared with controls. A diffuse uptake in the chest was also apparent, but the very intense uptake in the pelvis of these planar images and the poor resolution afforded by the planar imaging system hindered interpretation. The higher resolution capabilities afforded by a small-animal microPET imaging system with three-dimensional resolution capability should illuminate other sites of tumor involvement and permit direct comparison again to the gold standard for imaging non–Hodgkin's lymphoma, namely ^{18}F-FDG. However, these initial studies are already indicating a high level of sensitivity and specificity for pretargeted molecular imaging.

Conclusions

Highly specific and very sensitive images are possible with bsMAb pretargeting (73, 74, 85). Although the studies indicate that PET will likely outperform single-photon emission computed tomography–based imaging, it is important to note that the strong signal and high tumor/tissue ratios produce excellent image contrast even with conventional gamma scintillation cameras, and thus a pretargeting procedure based on a ^{99m}Tc-labeled peptide can be a useful and less expensive alternative to immunoPET. There are also other positron-emitting radionuclides with better PET imaging properties, such as ^{64}Cu or ^{68}Ga, that could also improve image quality with pretargeting. Thus, pretargeting with humanized bsMAbs seems to be an improvement over directly-labeled antibodies or fragments, and thus is a promising new molecular imaging method.

Acknowledgments

We thank M. Hernendez, J. Jebsen, T. Jackson, L. Muskova, L. Osorio, D. Yeldell for their technical assistance; and Drs. P. Zanzonico (Memorial Sloan-Kettering Cancer Center) and S. Vallabhajosula (Weill Medical College of Cornell University) for their contributions in the microPET imaging studies summarized herein.

References

1. Atri M. New technologies and directed agents for applications of cancer imaging. J Clin Oncol 2006; 24:3299–308.
2. Barentsz J, Takahashi S, Oyen W, et al. Commonly used imaging techniques for diagnosis and staging. J Clin Oncol 2006;24:3234–44.
3. Helms MW, Brandt BH, Contag CH. Options for visualizing metastatic disease in the living body. Contrib Microbiol 2006;13:209–31.
4. Schnall M, Rosen M. Primer on imaging technologies for cancer. J Clin Oncol 2006;24:3225–33.
5. Kelloff GJ, Krohn KA, Larson SM, et al. The progress and promise of molecular imaging probes in oncologic drug development. Clin Cancer Res 2005;11: 7967–85.
6. Kelloff GJ, Hoffman JM, Johnson B, et al. Progress and promise of FDG-PET imaging for cancer patient management and oncologic drug development. Clin Cancer Res 2005;11:2785–808.
7. Tsukamoto E, Ochi S. PET/CT today: system and its impact on cancer diagnosis. Ann Nucl Med 2006;20: 255–67.
8. Belhocine T, Spaepen K, Dusart M, et al. ^{18}FDG PET in oncology: the best and the worst [review]. Int J Oncol 2006;28:1249–61.
9. Divgi CR. Status of radiolabeled monoclonal antibodies for diagnosis and therapy of cancer. Oncology 1996;10:939–53.
10. Freeman LM, Krynyckyi BR, Li Y, et al. The role of ^{111}In Capromab Pendetide (Prosta-ScintR) immunoscintigraphy in the management of prostate cancer. Q J Nucl Med 2002;46:131–7.
11. Goldenberg DM. Perspectives on oncologic imaging with radiolabeled antibodies. Cancer 1997;80: 2431–5.
12. Goldenberg DM, Juweid M, Dunn RM, Sharkey RM. Cancer imaging with radiolabeled antibodies: new advances with technetium-99m-labeled monoclonal antibody Fab′ fragments, especially CEA-Scan and prospects for therapy. J Nucl Med Technol 1997;25: 18–23.
13. Moffat FL, Jr., Pinsky CM, Hammershaimb L, et al.; The Immunomedics Study Group. Clinical utility of external immunoscintigraphy with the IMMU-4 technetium-99m Fab′ antibody fragment in patients undergoing surgery for carcinoma of the colon and rectum: results of a pivotal, phase III trial. J Clin Oncol 1996;14:2295–305.
14. Sodee DB, Nelson AD, Faulhaber PF, Maclennan GT, Resnick MI, Bakale G. Update on fused capromab pendetide imaging of prostate cancer. Clin Prostate Cancer 2005;3:230–8.
15. Surwit EA, Childers JM, Krag DN, et al. Clinical assessment of ^{111}In-CYT-103 immunoscintigraphy in ovarian cancer. Gynecol Oncol 1993;48:285–92.
16. Lawrentschuk N, Davis ID, Bolton DM, Scott AM. Positron emission tomography and molecular imaging of the prostate: an update. BJU Int 2006;97:923–31.
17. Folkman J. Tumor angiogenesis: therapeutic implications. N Engl J Med 1971;285:1182–6.
18. Jain RK. Therapeutic implications of tumor physiology. Curr Opin Oncol 1991;3:1105–8.
19. Buchsbaum DJ. Experimental approaches to increase radiolabeled antibody localization in tumors. Cancer Res 1995;55:5729–32s.
20. Siegel JA, Pawlyk DA, Lee RE, et al. Tumor, red marrow, and organ dosimetry for ^{131}I-labeled anti-carcinoembryonic antigen monoclonal antibody. Cancer Res 1990;50:1039–42s.
21. Sharkey RM, Motta-Hennessy C, Pawlyk D, Siegel JA, Goldenberg DM. Biodistribution and radiation dose estimates for yttrium- and iodine-labeled monoclonal antibody IgG and fragments in nude mice bearing human colonic tumor xenografts. Cancer Res 1990;50:2330–6.
22. Behr TM, Sharkey RM, Juweid ME, et al. Reduction of the renal uptake of radiolabeled monoclonal antibody fragments by cationic amino acids and their derivatives. Cancer Res 1995;55:3825–34.
23. Colcher D, Pavlinkova G, Beresford G, Booth BJ, Choudhury A, Batra SK. Pharmacokinetics and biodistribution of genetically-engineered antibodies. Q J Nucl Med 1998;42:225–41.
24. Cosman M, Krishnan VV, Balhorn R. Application of NMR methods to identify detection reagents for use in development of robust nanosensors. Methods Mol Biol 2005;300:141–63.
25. Cortez-Retamozo V, Backmann N, Senter PD, et al. Efficient cancer therapy with a nanobody-based conjugate. Cancer Res 2004;64:2853–7.
26. Wahlberg E, Lendel C, Helgstrand M, et al. An affibody in complex with a target protein: structure and coupled folding. Proc Natl Acad Sci U S A 2003;100: 3185–90.
27. Slavin-Chiorini DC, Horan Hand PH, Kashmiri SV, Calvo B, Zaremba S, Schlom J. Biologic properties of a CH2 domain-deleted recombinant immunoglobulin. Int J Cancer 1993;53:97–103.
28. Kenanova V, Olafsen T, Crow DM, et al. Tailoring the pharmacokinetics and positron emission tomography imaging properties of anti-carcinoembryonic antigen single-chain Fv-Fc antibody fragments. Cancer Res 2005;65:622–31.
29. Olafsen T, Kenanova VE, Sundaresan G, et al. Optimizing radiolabeled engineered antip185HER2 antibody fragments for *in vivo* imaging. Cancer Res 2005;65:5907–16.
30. Wu AM. Engineering multivalent antibody fragments for *in vivo* targeting. Methods Mol Biol 2004; 248:209–25.
31. Binz HK, Amstutz P, Pluckthun A. Engineering novel binding proteins from nonimmunoglobulin domains. Nat Biotechnol 2005;23:1257–68.
32. Anderson CJ. Metabolism of radiometal-labeled proteins and peptides: what are the real radiopharmaceuticals *in vivo*? Cancer Biother Radiopharm 2001; 16:451–5.
33. Anderson WT, Strand M. Radiolabeled antibody: iodine versus radiometal chelates. NCI Monogr 1987; 3:149–51.
34. Ando A, Ando I. Tumor uptake and biodistribution of various radiolabels. Acta Radiol Suppl 1990;374: 65–74.
35. Larson SM. Mechanisms of localization of gallium-67 in tumors. Semin Nucl Med 1978;8:193–203.
36. Scheinberg DA, Strand M. Kinetic and catabolic considerations of monoclonal antibody targeting in erythroleukemic mice. Cancer Res 1983;43:265–72.
37. Michel RB, Ochakovskaya R, Mattes MJ. Antibody localization to B-cell lymphoma xenografts in immunodeficient mice: importance of using residualizing radiolabels. Clin Cancer Res 2002;8:2632–9.
38. Stein R, Govindan SV, Mattes MJ, et al. Targeting human cancer xenografts with monoclonal antibodies labeled using radioiodinated, diethylenetriaminepentaacetic acid-appended peptides. Clin Cancer Res 1999;5:3079–87s.
39. Wong JY, Chu DZ, Williams LE, et al. Pilot trial evaluating an ^{123}I-labeled 80-kilodalton engineered anti-carcinoembryonic antigen antibody fragment (cT84.66 minibody) in patients with colorectal cancer. Clin Cancer Res 2004;10:5014–21.
40. Kalofonos HP, Karamouzis MV, Epenetos AA. Radioimmunoscintigraphy in patients with ovarian cancer. Acta Oncol 2001;40:549–57.
41. Goldenberg DM, Wlodkowski TJ, Sharkey RM, et al. Colorectal cancer imaging with iodine-123-labeled

CEA monoclonal antibody fragments. J Nucl Med 1993;34:61–70.
42. Bischof-Delaloye A, Delaloye B, Buchegger F, et al. Clinical value of immunoscintigraphy in colorectal carcinoma patients: a prospective study. J Nucl Med 1989;30:1646–56.
43. Zalutsky MR. Potential of immuno-positron emission tomography for tumor imaging and immunotherapy planning. Clin Cancer Res 2006;12:1958–60.
44. Kairemo KJ. Positron emission tomography of monoclonal antibodies. Acta Oncol 1993;32:825–30.
45. Bakir MA, Eccles S, Babich JW, et al. c-erbB2 protein overexpression in breast cancer as a target for PET using iodine-124-labeled monoclonal antibodies. J Nucl Med 1992;33:2154–60.
46. Larson SM, Pentlow KS, Volkow ND, et al. PET scanning of iodine-124-3F9 as an approach to tumor dosimetry during treatment planning for radioimmunotherapy in a child with neuroblastoma. J Nucl Med 1992;33:2020–3.
47. Sundaresan G, Yazaki PJ, Shively JE, et al. ^{124}I-labeled engineered anti-CEA minibodies and diabodies allow high-contrast, antigen-specific small-animal PET imaging of xenografts in athymic mice. J Nucl Med 2003;44:1962–9.
48. Robinson MK, Doss M, Shaller C, et al. Quantitative immuno-positron emission tomography imaging of HER2-positive tumor xenografts with an iodine-124 labeled anti-HER2 diabody. Cancer Res 2005;65: 1471–8.
49. Grunberg J, Novak-Hofer I, Honer M, et al. *In vivo* evaluation of ^{177}Lu- and $^{67/64}$Cu-labeled recombinant fragments of antibody chCE7 for radioimmunotherapy and PET imaging of L1-CAM-positive tumors. Clin Cancer Res 2005;11:5112–20.
50. Lewis MR, Wang M, Axworthy DB, et al. *In vivo* evaluation of pretargeted ^{64}Cu for tumor imaging and therapy. J Nucl Med 2003;44:1284–92.
51. Yazaki PJ, Wu AM, Tsai SW, et al. Tumor targeting of radiometal labeled anti-CEA recombinant T84.66 diabody and t84.66 minibody: comparison to radioiodinated fragments. Bioconjug Chem 2001;12:220–8.
52. Abdel-Nabi HH, Chan HW, Doerr RJ. Indium-labeled anti-colorectal carcinoma monoclonal antibody accumulation in non-tumored tissue in patients with colorectal carcinoma. J Nucl Med 1990;31: 1975–9.
53. Abdel-Nabi HH, Schwartz AN, Higano CS, Wechter DG, Unger MW. Colorectal carcinoma: detection with indium-111 anticarcinoembryonic-antigen monoclonal antibody ZCE025. Radiology 1987;164:617–21.
54. DeNardo GL, DeNardo SJ. Evaluation of a cathepsin-cleavable peptide linked radioimmunoconjugate of a panadenocarcinoma MAb, m170, in mice and patients. Cancer Biother Radiopharm 2004;19: 85–92.
55. van Eerd JE, Vegt E, Wetzels JF, et al. Gelatin-based plasma expander effectively reduces renal uptake of ^{111}In-octreotide in mice and rats. J Nucl Med 2006; 47:528–33.
56. Vegt E, Wetzels JF, Russel FG, et al. Renal uptake of radiolabeled octreotide in human subjects is efficiently inhibited by succinylated gelatin. J Nucl Med 2006; 47:432–6.
57. Bodei L, Cremonesi M, Zoboli S, et al. Receptor-mediated radionuclide therapy with ^{90}YDOTATOC in association with amino acid infusion: a phase I study. Eur J Nucl Med Mol Imaging 2003;30:207–16.
58. Chauhan SC, Jain M, Moore ED, et al. Pharmacokinetics and biodistribution of ^{177}Lu-labeled multivalent single-chain Fv construct of the pancarcinoma monoclonal antibody CC49. Eur J Nucl Med Mol Imaging 2005;32:264–73.
59. Wittel UA, Jain M, Goel A, Chauhan SC, Colcher D, Batra SK. The *in vivo* characteristics of genetically engineered divalent and tetravalent single-chain antibody constructs. Nucl Med Biol 2005;32:157–64.
60. Batra SK, Jain M, Wittel UA, Chauhan SC, Colcher D. Pharmacokinetics and biodistribution of genetically engineered antibodies. Curr Opin Biotechnol 2002;13: 603–8.
61. Goodwin DA, Meares CF, David GF, et al. Monoclonal antibodies as reversible equilibrium carriers of radiopharmaceuticals. Int J Radiat Appl Instrum Part B 1986;13:383–91.
62. Reardan DT, Meares CF, Goodwin DA, et al. Antibodies against metal chelates. Nature 1985;316: 265–8.
63. Rossi EA, Goldenberg DM, Cardillo TM, McBride WJ, Sharkey RM, Chang CH. Stably tethered multifunctional structures of defined composition made by the dock and lock method for use in cancer targeting. Proc Natl Acad Sci U S A 2006;103:6841–6.
64. Rossi EA, Chang CH, Losman MJ, et al. Pretargeting of carcinoembryonic antigen-expressing cancers with a trivalent bispecific fusion protein produced in myeloma cells. Clin Cancer Res 2005;11:7122–9s.
65. Rossi EA, Sharkey RM, McBride W, et al. Development of new multivalent-bispecific agents for pretargeting tumor localization and therapy. Clin Cancer Res 2003;9:3886–96S.
66. Stickney DR, Anderson LD, Slater JB, et al. Bifunctional antibody: a binary radiopharmaceutical delivery system for imaging colorectal carcinoma. Cancer Res 1991;51:6650–5.
67. Patt YZ, Lamki LM, Shanken J, et al. Imaging with indium111-labeled anticarcinoembryonic antigen monoclonal antibody ZCE-025 of recurrent colorectal or carcinoembryonic antigen-producing cancer in patients with rising serum carcinoembryonic antigen levels and occult metastases. J Clin Oncol 1990;8: 1246–54.
68. Lamki LM, Patt YZ, Rosenblum MG, et al. Metastatic colorectal cancer: radioimmunoscintigraphy with a stabilized In-111-labeled F(ab')2 fragment of an anti-CEA monoclonal antibody. Radiology 1990; 174:147–51.
69. Le Doussal JM, Martin M, Gautherot E, Delaage M, Barbet J. *In vitro* and *in vivo* targeting of radiolabeled monovalent and divalent haptens with dual specificity monoclonal antibody conjugates: enhanced divalent hapten affinity for cell-bound antibody conjugate. J Nucl Med 1989;30:1358–66.
70. Boerman OC, Kranenborg MH, Oosterwijk E, et al. Pretargeting of renal cell carcinoma: improved tumor targeting with a bivalent chelate. Cancer Res 1999; 59:4400–5.
71. Goodwin DA, Meares CF, Watanabe N, et al. Pharmacokinetics of pretargeted monoclonal antibody 2D12.5 and ^{88}Y-Janus-2-(*p*-nitrobenzyl)-1,4,7,10-tetraazacyclododecanetetraacetic acid (DOTA) in BALB/c mice with KHJJ mouse adenocarcinoma: a model for ^{90}Y radioimmunotherapy. Cancer Res 1994; 54:5937–46.
72. Chetanneau A, Barbet J, Peltier P, et al. Pretargetted imaging of colorectal cancer recurrences using an ^{111}In-labelled bivalent hapten and a bispecific antibody conjugate. Nucl Med Commun 1994;15: 972–80.
73. Le Doussal JM, Chetanneau A, Gruaz-Guyon A, et al. Bispecific monoclonal antibody-mediated targeting of an indium-111-labeled DTPA dimer to primary colorectal tumors: pharmacokinetics, biodistribution, scintigraphy and immune response. J Nucl Med 1993; 34:1662–71.
74. Peltier P, Curtet C, Chatal JF, et al. Radioimmunodetection of medullary thyroid cancer using a bispecific anti-CEA/anti-indium-DTPA antibody and an indium-111-labeled DTPA dimer. J Nucl Med 1993; 34:1267–73.
75. McBride WJ, Zanzonico P, Sharkey RM, et al. Bispecific antibody pretargeting PET (ImmunoPET) with an ^{124}I-labeled hapten-peptide. J Nucl Med 2006;47: 1678–88.
76. Sharkey RM, Cardillo TM, Rossi EA, et al. Signal amplification in molecular imaging by pretargeting a multivalent, bispecific antibody. Nat Med 2005;11: 1250–5.
77. Karacay H, Sharkey RM, McBride WJ, et al. Pretargeting for cancer radioimmunotherapy with bispecific antibodies: role of the bispecific antibody's valency for the tumor target antigen. Bioconjug Chem 2002; 13:1054–70.
78. Sharkey RM, McBride WJ, Karacay H, et al. A universal pretargeting system for cancer detection and therapy using bispecific antibody. Cancer Res 2003; 63:354–63.
79. Griffiths GL, Chang CH, McBride WJ, et al. Reagents and methods for PET using bispecific antibody pretargeting and ^{68}Ga-radiolabeled bivalent hapten-peptide-chelate conjugates. J Nucl Med 2004;45:30–9.
80. Sharkey RM, Weadock KS, Natale A, et al. Successful radioimmunotherapy for lung metastasis of human colonic cancer in nude mice. J Natl Cancer Inst 1991; 83:627–32.
81. Sharkey RM, Karacay H, Vallabhajosula S, et al. Molecular imaging with pretargeted ImmunoSPECT and ImmunoPET in a model of metastatic colon carcinoma. Radiol. In press 2007.
82. Cardillo TM, Karacay H, Goldenberg DM, et al. Improved targeting of pancreatic cancer: experimental studies of a new bispecific antibody, pretargeting enhancement system for immunoscintigraphy. Clin Cancer Res 2004;10:3552–61.
83. Sharkey RM, Karacay H, Chang CH, McBride WJ, Horak ID, Goldenberg DM. Improved therapy of non-Hodgkin's lymphoma xenografts using radionuclides pretargeted with a new anti-CD20 bispecific antibody. Leukemia 2005;19:1064–9.
84. Ghetie MA, Richardson J, Tucker T, Jones D, Uhr JW, Vitetta ES. Disseminated or localized growth of a human B-cell tumor (Daudi) in SCID mice. Int J Cancer 1990;45:481–5.
85. Goldenberg DM, Sharkey RM, Paganelli G, Barbet J, Chatal JF. Antibody pretargeting advances cancer radioimmunodetection and radioimmunotherapy. J Clin Oncol 2006;24:823–34.